Journal Materials Chemistry A

ROYAL SOCIETY OF CHEMISTRY

ARTICLE

Visible light photocatalysis by metal-to-metal charge transfer for degradation of methyl orange

C. P. Ireland,[a] R. G. Palgrave,[b] S. C. Bennett,[c] A. W. J. Smith,[c] J. H. Clark,[a] J. R. Darwent,[a] J. B. Claridge,[a] S. Poulston,[c] and M. J. Rosseinsky[a]

We have impregnated chromium (III) onto a high surface area particulate niobium oxide to make bulk oxide-oxide interfaces, identifying by a combination of X-ray Photoelectron Spectroscopy and diffuse reflectance the exact energy of the metal-to-metal charge transfer transition that is responsible for the visible light photocatalytic decomposition of methyl orange.

1. Introduction

The harvesting of visible light to carry out photochemical transformations is attractive for solar fuel, antimicrobial and depollution applications.[1-4] Oxide materials are attractive photocatalysts but often have band gaps that are in the ultra violet region of the spectrum due to the position of the O $2p$ valence band derived from the electronegative oxide anion.[5-7] The fundamental inter-band transition in d^0 transition metal oxides typically has anion (valence band) to metal (conduction band) character. Materials with a mixture of d^n and d^0 cations (n>0) can absorb light by a metal-to-metal charge transfer mechanism *e.g.* by Cu^+ to Zr^{4+},[8] Cr^{3+} to Ti^{4+} in grafted systems,[9, 10] and Cu^{2+} to Ti^{4+} in crystalline ordered multiple sub lattice systems.[11] For example, Cr^{3+} bound to rutile TiO_2 produces visible light absorption due to both $d-d$ transitions from the open shell cation and the metal-to-metal charge transfer transitions, which were assessed to occur in the visible range (less than 3 eV) because of the pH 7 conduction band position of rutile (-0.4 V) and the 2.1 V position of the $Cr^{3+/4+}$ redox couple,[9] permitting decomposition of 2-propanol into carbon dioxide and acetone under visible light. Although not as well studied as titanium oxide, niobium oxide is also an active ultraviolet photocatalyst, with a bulk band gap of 3.4 eV.[12] Kominami *et al*[13] synthesised niobium oxide from a solvothermal synthesis route, producing hydrogen from a methanol solution with and without a platinum co-catalyst; using mesoporous niobium oxide synthesised via a templating route, Chen *et al*[14] generated hydrogen from methanol solution when the mesoporous niobium oxide a platinum co-catalyst, and Prado's group use niobium oxide based photocatalysts for indigo carmine dye degradation reactions.[15-17] Inducing visible light activity in UV active material such as niobium oxide can be achieved by cation or anion doping, or adding a sensitizer. Ge et al. sensitized the surface of niobium oxide by adding a surface carbonate species, successfully generating hydrogen from a water/methanol solution under visible light.[18] Wang et al. sensitized a nitrogen doped niobium oxide material with a carbon nitride polymer, again inducing visible light absorbance, degrading the dye Rhodium B under visible light.[19] In this paper we impregnate Cr^{3+} onto a high surface area particulate niobium oxide to make bulk oxide-oxide interfaces and identify by a combination of spectroscopies the exact energy of the metal-to-metal charge transfer transition that is responsible for the visible light photocatalytic decomposition of methyl orange.

2. Experimental

2.1 Synthetic procedures

2.1.1 Niobium oxide synthesis. 150 g (0.6 mol) of $NbCl_5$ was added slowly to 1.2 L of anhydrous EtOH at room temperature, generating a clear yellow/green 0.5 M solution of $NbCl_5$. This solution was added to 6 L of a previously prepared 0.55 M solution of NH_3, under vigorous stirring, using a peristaltic pump, set to a rate of 20 ml min^{-1}. A white precipitate was formed on addition of the $NbCl_5$ solution. At the conclusion of the addition, the suspension was allowed to stir for a further hour, before the precipitate material was collected by filtration, by transferring the suspension to a filter funnel under vacuum. This white precipitate material was continuously washed with deionized water heated to a temperature of 60 °C, until the conductivity of the washings collected showed conductivity of less than 50 μS, as measured

[a.] Department of Chemistry, University of Liverpool, Liverpool, UK L69 7ZD. E-mail: m.j.rosseinsky@liv.ac.uk; Fax: +44 (0)151 794 3587; Tel: +44 (0)151 794 3499.
[b.] Current address: Department of Chemistry, University College London, Christopher Ingold Laboratories, 20 Gordon Street, London, WC1H 0AJ, U.K..
[c.] Johnson Matthey Technology Centre, Blounts Court, Sonning Common, Reading RG4 9NH, U.K.

by a conductivity meter. This material was then further washed with 2 L of deionized water, and collected and dried overnight in an oven at 105 °C. The material was ground into a fine white powder and calcined in a furnace at 500 °C for 2 hours, heating at 5 °C min^{-1} and cooling at 10 °C min^{-1}.

2.1.2 Chromium impregnated material. 10 g of Nb_2O_5 was impregnated with 2.30 ml of 2.5 M chromium (III) nitrate solution, and 1.70 ml of water to bring the solution up to the incipient wetness point (0.4 ml g^{-1}). This material was then dried in an oven overnight at 105 °C then calcined in air at 500 °C for 2 hours, heating at 5 °C min^{-1}, and cooling at 10 °C min^{-1} to afford 3% chromium by weight impregnated onto Nb_2O_5. 0.8 g of this as made material was then placed in 400 ml distilled water under constant stirring for 2 hours, allowing chromium (VI) to leech out into the water. The material was collected by centrifuge at 2500 rpm, and the UV/Vis absorbance of the washing was measured from 240 nm to 600 nm, to determine the chromate content. The collected material was placed in 200 ml of distilled water, and stirred for 30 minutes. Again the material was collected by centrifuge at 2500 rpm, and the chromate content of the washing determined by UV/Vis; this washing procedure continued until no evidence of chromate was detected by UV/Vis absorbance. This final washed product (3%Cr_2O_3-Nb_2O_5), collected by centrifuge, was dried overnight in an oven at 105 °C. 1% by weight chromium (1%Cr_2O_3-Nb_2O_5) and 5% by weight chromium (5%Cr_2O_3-Nb_2O_5) composites were similarly prepared by varying the amount of chromium nitrate dissolved in water in the initial stage of the synthesis. For comparison, 1.5 g of the initial impregnated sample was calcined at lower temperature (350 °C) in air; 1.5 g of the material was calcined in a nitrogen atmosphere at 350 °C.

2.1.3 Methyl orange preparation. A 0.010 M acetate buffer solution was prepared, by dissolving 0.5685 g of acetic acid, and 0.0725 g of sodium acetate in 1 L of deionized water (pH 6.9), to generate a pH 3.5 buffer solution. A pH meter confirmed the pH of this buffer solution to be 3.50. UV/Vis spectroscopy of this clear buffer solution shows no absorbance between the range 240 to 700 nm. To this 1 L solution, 0.02 g of methyl orange was added, producing the protonated form of methyl orange, with its characteristic red colour (6.11 x 10^{-5} M methyl orange), with the maximum absorbance of the buffered methyl orange solution occurring at 495 nm. This solution was stable for a period of months, with no loss in concentration.

2.2 Characterisation

2.2.1 5 point BET surface area. This was determined using a Quantachrome Nova Gas sorption analyser. In a typical analysis, 0.20 g of material was placed in a reactor, set up to degas at a temperature of 105 °C overnight. After degassing, the reactor was placed in the sorption analyser, with nitrogen as the sorption gas, and the BET isotherm measured at 5 points along the linear section of the full adsorbance isotherm (p/p$_0$ = 0.05 to 0.35). The volume of a monolayer of nitrogen adsorbed onto the available surface of the sample was

calculated from the BET theory expression, and the surface area was calculated from this value.

2.2.2 The diffuse reflectance spectra were obtained using a Perkin-Elmer Lambda 650 S UV/vis spectrometer equipped with a Labsphere integrating sphere over the spectral range 190-900 nm, using $BaSO_4$ reflectance standards. The spectra were analysed by using the Kubelka-Munk function, $F(R)=(1-R)2/2R = K/S$, with K the absorption and S the scattering coefficient, to represent the absorption coefficient of the sample. The indirect band gap calculations were determined by plotting $(F(R)xE)^{1/2}$ vs E, with F(R) determined from the reflectance as described.

2.2.3 X-ray photoelectron spectroscopy (XPS) was carried out on a Scienta ESCA 300 spectrometer located at the NCESS facility at Daresbury Laboratory, UK, which incorporated a rotating anode Al Kα (hν = 1486.6 eV) X-ray source and had an effective instrument resolution of 400 meV. The spectrometer was calibrated regularly to set the Fermi edge of a silver reference sample at zero binging energy. Sample charging was compensated for using an electron flood gun. The binding energy scale was referenced using the adventitious carbon C1s peak which was set to 284.6 eV.

2.2.4 Methyl orange degradation reactions were carried out under a 300W Xe Oriel lamp, with a 420 nm cut off filter, and an IR water filter. In a typical reaction, 100 ml of the methyl orange solution was placed in a Pyrex reactor, along with 0.1 g of catalyst. Oxygen was bubbled in the reactor at a constant rate to ensure the reaction suspension was continually saturated with oxygen. Typically the reaction suspension was allowed to equilibrate in the dark under oxygen for one hour. The reaction was initiated by turning on the lamp. At points in the reaction, the light was turned off, and approximately 8 ml of sample was removed from the reactor. The catalyst was filtered from the reaction using 0.2 μm GMP membrane filters, and 3 x 2 ml samples were measured by UV/Vis spectroscopy, using a Perkin-Elmer Lambda 650 S UV/vis spectrometer. A 1 cm path length cell was used, and the spectrum was measured from 240 nm – 700 nm. The absorbance at wavelength 495 nm was noted, with three measurements averaged. The methyl orange solution was then recombined with the catalyst filtered out from the reactor, and this suspension was placed back in the reactor; the light was then turned on, and the reaction continued. The pH was monitored throughout, and found to be at a pH of 3.50 ± 0.05 throughout all degradation reactions.

2.2.5 The moles of photons incident on the reactor at 400 nm and 450 nm were carried out by Potassium Ferrioxalate Chemical actinometry,[20] using the 300 W Xe lamp with band pass filters centred at 400 nm and 450 nm. The calculations gave values of 1.15 x 10^{20} photons h^{-1} at 400 nm, and 2.10 x 10^{20} photons h^{-1} at 450 nm. By using these values with moles of methyl orange degraded per unit time the quantum efficiency, of these reactions at each wavelength can be calculated, and plotted in an action spectrum.

2.2.6 X-ray diffraction was carried out on a Panalytical X'pert Pro diffractometer with a cobalt radiation source. SEM imaging

was carried out on a Hitachi S-4800 scanning electron microscope. TEM imaging was carried out on a JEOL 2100F transmission electron microscope, operating at 200 kV (Cs aberration corrected).

3 Results and Discussion

3.1 Synthesis of material

The Nb_2O_5 support showed a semi-amorphous structure with broad peaks that correspond to the pseudo-hexagonal phase of Nb_2O_5 (Figure S1) and has a BET surface area of 129 m^2 g^{-1}. Assuming spherical particles, from the surface area the average particle diameter can be estimated to be 10 nm. Microscopy images confirm agglomerated particles approximately 10 nm in size (Figure S2). The direct band gap was calculated to be 3.59 eV from the diffuse reflectance (Figure S3). The analysed N content was 0% and the H content 0.59%. Both chlorine ICP analysis and XPS confirm undetectable levels of chlorine present after the synthesis.

Figure S4 illustrates the TGA data for the material after Nb_2O_5 is impregnated with the chromium (III) nitrate solution and dried ($3\%Cr(NO_3)_3$-Nb_2O_5). CHN analysis shows nitrogen is present, from surface chromium nitrate. The nitrate decomposes with increasing temperature. CHN analysis of the post – calcined material ($3\%CrO_x$-Nb_2O_5) confirms the nitrate removal.

The X-ray diffraction pattern of $3\%CrO_x$-Nb_2O_5 is shown in Figure S1, in addition to XRD data of the Nb_2O_5 used in the synthesis. There is no evidence from XRD of a crystalline chromium oxide species in the composite, when compared to the XRD of Nb_2O_5; the two X-ray diffraction patterns are the same. The BET surface area of the composite was calculated to be 110 m^2 g^{-1}, comparable to the surface area of the Nb_2O_5 starting material (129 m^2 g^{-1}). Xie and Tang discussed the spontaneous monolayer dispersion of oxides and salts onto supports.[21] They noted that at low loadings of oxides onto supports, there is no evidence of the oxide in XRD patterns. As the weight of loading increases, evidence of the oxide appears in the form of crystalline peaks in the X-ray of the material. The point at which this change occurs corresponds to the oxide addition forming a complete monolayer on the surface of the support. Xie and Tang assume the O^{2-} ions of the loaded oxide form a close packed layer on the surface of the support; by using the radius of an O^{2-} ion, the amount of loaded oxide required to form a monolayer on the surface can be calculated, which would require 11% by weight of chromium in this case. From the weight of chromium added, and the BET surface area of the material, there are 0.45 monolayers of CrO_x for the $5\%CrO_x$-Nb_2O_5, 0.27 monolayers for $3\%CrO_x$-Nb_2O_5 and 0.09 monolayers for $1\%CrO_x$-Nb_2O_5.

3.2 Oxidation state of chromium in the material

XPS was used to determine the oxidation state of the chromium throughout the synthesis procedure. Cr(III), as a d^3 cation, shows photoemission core lines with multiplet splitting which are unresolved using the present spectrometer. Therefore, the Cr 2p core line for $3\%Cr(NO_3)_3$-Nb_2O_5 is asymmetric (Figure 1a), in common with spectra from Cr_2O_3. In contrast, Cr(VI) is a d^0 ion so we would expect no multiplet slitting and therefore a symmetrical Cr 2p coreline. Since the object of the analysis is to determine

Cr(III):Cr(VI) ratio, no attempt was made to model the individual multlplet components of the Cr(III) peak. Instead, each spin orbit component of the Cr(III) peak was fitted with a single Gaussian-Lorentzian peak with an added exponential term to provide a tail on the high binding energy side. The areas of the spin orbit components were constrained to the expected 2:1 ratio. Cr(VI) peaks were fitted with symmetrical Gaussian-Lorentzian components. In $3\%Cr(NO_3)_3$-Nb_2O_5, the Cr $2p_{3/2}$ peak maximum is present at a binding energy of 577.5 eV (Figure 1a). After calcination in air, a higher binding energy component is seen, which can be fitted with a symmetrical peak at a binding energy of 579.3 eV, corresponding to Cr(VI) (Figure 1b). The Cr(III) component also shifts down slightly in binding energy to 576.5 eV; this change may represent decomposition of the nitrate to form an oxide phase.
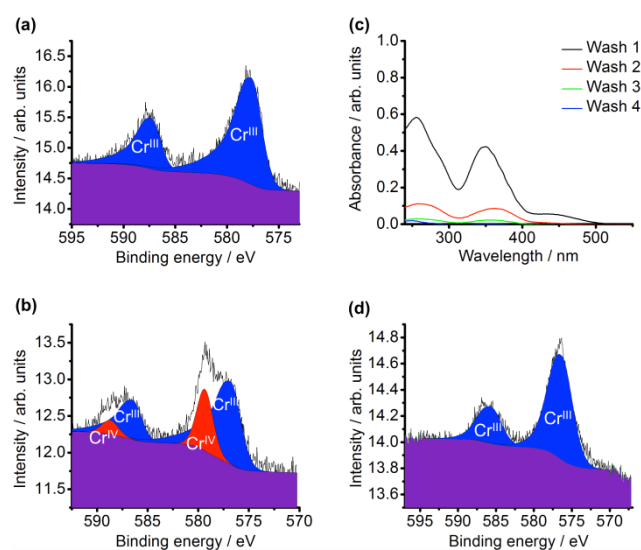

Fig 1 a) XPS data of $3\%Cr(NO_3)_3$-Nb_2O_5, with fitted chromium (III) XPS peaks. (b) XPS data of $3\%CrO_x$-Nb_2O_5, with fitted chromium (III) and chromium (VI) peaks. (c) UV Vis absorbance spectra of $3\%CrO_x$-Nb_2O_5 washings; the intensity of the chromium (VI) absorbance peaks decreasing until undetectable by UV/Vis spectroscopy after 4 consecutive washes. (d) XPS data of $3\%Cr_2O_3$-Nb_2O_5 after washing, with fitted chromium (III) XPS peaks.

When $3\%Cr(NO_3)_3$-Nb_2O_5 is calcined in a nitrogen atmosphere, as opposed to air, Cr(VI) was still present, but in lower concentration, indicating that the source of the oxidizing agent must be in part from the products of the decomposition of the nitrate to the oxide in addition to atmospheric oxygen. Table 1 shows the amount of Cr(VI) produced after calcination under different conditions.

Further evidence for the detection of chromate can be found by stirring the $3\%CrO_x$-Nb_2O_5 composite in deionized water for two hours; the UV/Vis spectrum of the recovered water can be measured. The spectrum, (Figure 1c) with significant peaks centered at 256 nm and 350 nm, is characteristic of chromium (VI) as $Cr_2O_7^{2-}$, indicating that chromium (VI) is leaching out of the composite.[22] If this process is repeated, essentially washing the material, a significant decrease in intensity of the chromium (VI) peak can be observed in the washings, indicating chromium (VI) is being removed from the $3\%CrO_x$-Nb_2O_5. By repeating this cycle an additional three times, the amount of chromate leaching out of the catalyst into the deionized water becomes undetectable by UV/Vis

spectroscopy with the absorbance at the chromium (VI) peak at 371 nm indicating a $Cr_2O_7^{2-}$ concentration of less than 2×10^{-7} mol l^{-1}. (Figure 1c). XPS confirms this is the case; after the washing procedure, the Cr(VI) component in the XPS spectrum is completely removed, and only the Cr(III) component remains, with a binding energy of 576.9 eV. (Figure 1d).

XPS was used to calculate the Cr:Nb surface ratios at each stage of the synthesis procedure. $3\%Cr(NO_3)_3$-Nb_2O_5 has a nominal molar Cr:Nb ratio of 0.054. The measured surface Cr:Nb ratio after $Cr(NO_3)_3$ impregnation was 0.11, showing a significant enhancement over the nominal value due to surface localization of the Cr species. After calcining, the Cr:Nb ratio was unchanged within experimental error. After washing, the Cr:Nb surface ratio reduced to 0.05, showing that around half of the Cr had been removed compared to the initial impregnation.

Calcination Conditions	Cr III / %	Cr VI / %
500 °C, air	72	28
350 °C, air	43	57
350 °C, N_2	68	32

Table 1 Ratio of the oxidation state of 3% CrO_x-Nb_2O_5 after calcination under various conditions

Microscopy images of the $5\%Cr_2O_3$-Nb_2O_5 material show a comparable morphology to the Nb_2O_5 starting material, with agglomerate particles approximately 10 nm in size (Figure S5). EDX mapping shows an even distribution of chromium across the agglomerate particles (Figure S6), with a ratio of 21:79 Cr:Nb measured on the surface. Separate particles of CrO_x were not observed. The coverage of chromium on the niobium oxide particles is consistent with the material before washing ($5\%CrO_x$-Nb_2O_5) having 0.45 monolayers of chromium, with approximately half the chromium removed during the washing procedure.

3.3 Optical properties of the material

The evolution of the optical properties, and the colour of the material as the thermal treatment of the catalyst develops, is shown in Figure 2a and 2b-e respectively.

As the composite material is synthesized from Nb_2O_5, the material changes colour from the white of Nb_2O_5, (Figure 2b) through to the green of the final washed composite, $3\%Cr_2O_3$-Nb_2O_5 (Figure 2e). The diffuse reflectance of $3\%Cr(NO_3)_3$-Nb_2O_5 is dominated by the Nb_2O_5 band gap at 3.6 eV. The visible absorbance seen between 1.3 and 3 eV can be accounted for by the $d - d$ transitions of Cr^{3+}. In this pre calcination material, there is no evidence of charge transfer between the chromium and niobium species. An absorption peak at 6 eV in this spectrum is too high in energy to be a $d - d$ transition and appears only in spectra of $Cr(NO3)_3$ containing samples, and so is assigned to a higher energy transition originating from $Cr(NO_3)_3$.

When $3\%Cr(NO_3)_3$-Nb_2O_5 is calcined at 500°C in air, the optical properties change significantly. The colour changes from green (Figure 2c), to dark yellow (Figure 2d), and the diffuse reflectance of $3\%CrO_x$-Nb_2O_5 now shows significant visible absorption, although the Nb_2O_5 band gap is still evident. It is noticeable that there is a redshift of about 0.1 eV of this band edge feature in $3\%CrO_x$-Nb_2O_5 compared to Nb_2O_5. As shown

above, XPS of this material shows chromium present as both chromium (III) and chromium (VI) (Figure 1b); solutions of chromium (VI) compounds have a characteristic spectrum, with absorbance in the UV region centred around 275 nm (4.5 eV) and 375 nm (3.3 eV).[22] The diffuse reflectance of $3\%CrO_x$-Nb_2O_5 shows a hump and shoulder between 2.1 eV and 3.5 eV. This feature, which is absent pre-calcination, concurs with the XPS data by indicating chromium (III), chromium (VI) transitions. The hump around 3.1 eV is indicative of chromium (VI) absorbance by oxygen to chromium charge transfer, as noted by Shen and Guo, who observed these transitions in the UV/Vis spectrum of chromium and titanium co-incorporated onto MCM-41.[23] As shown in Figure 1c, washing removes the chromium (VI) species, the XPS shows chromium present in the +3 oxidation state only, and the diffuse reflectance of this final washed product $3\%Cr_2O_3$-Nb_2O_5 shows a decreased intensity where the chromium (VI) transition was occurring. In the absence of chromium (VI) for the samples after washing, the absorbance evident in the diffuse reflectance is therefore due to the Nb_2O_5 and Cr_2O_3 on the surface of the Nb_2O_5, together with any interaction between the chromium (III) and niobium (V) ions i.e. MMCT between the two ions. The final product absorbs in the visible region, unlike the Nb_2O_5 support starting material.
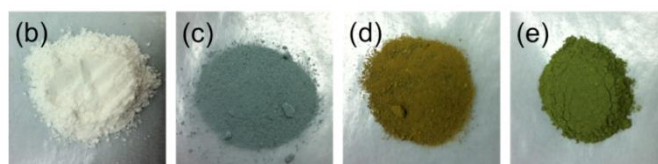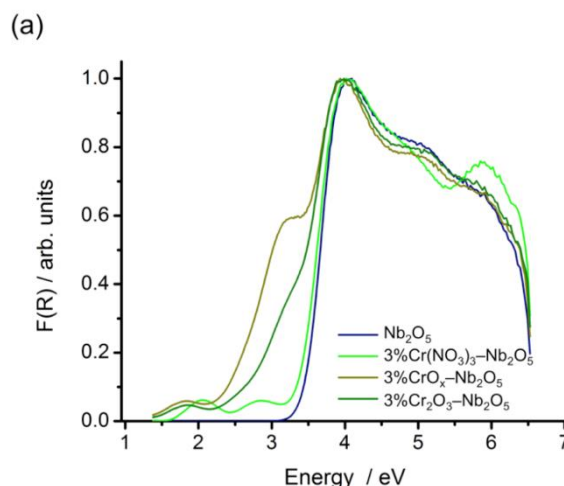

Fig 2 The diffuse reflectance spectra, (a) and photographs of the composite at different stages of the synthesis: (b) Nb_2O_5, (c) $3\%Cr(NO_3)_3$-Nb_2O_5, (d) $3\%CrO_x$-Nb_2O_5, e) $3\%Cr_2O_3$-Nb_2O_5.

By normalizing to the maximum absorbance the diffuse reflectance spectrum of Nb_2O_5, Cr_2O_3 and $3\%Cr_2O_3$-Nb_2O_5, the spectrum of the three materials can be compared (Figure 3a), and the difference between the three spectra, noticeably in the visible region, can be seen. By subtracting the measured Nb_2O_5 diffuse reflectance from that of $3\%Cr_2O_3$-Nb_2O_5, the

difference between the two, highlighting the visible absorbance, can be seen more clearly (Figure 3b). In this difference spectrum, optical absorption solely from the Nb_2O_5 phase is removed, leaving contributions only from Cr_2O_3 and potentially also from processes involving both Cr_2O_3 and Nb_2O_5. To isolate these absorption involving both Cr_2O_3 and Nb_2O_5, those arising from Cr_2O_3 alone must also be subtracted. Octahedral chromium (III) has three spin allowed electronic transitions from the $^4A_{2g}$ ground state. In the optical spectrum of Cr_2O_3 (Figure 3a) the first two transitions are clearly seen at 2.01 eV ($^4A_{2g} \rightarrow {}^4T_{2g}$) and 2.62 eV ($^4A_{2g} \rightarrow {}^4T_{1g}$). The third transition ($^4A_{2g} \rightarrow {}^4T_{1g}$) is obscured by the onset of LMCT transitions around 3.3 eV, but from Tanabe-Sugano diagrams is expected around 4.2 eV. The difference spectrum (Figure 3b) shows features characteristic of chromium (III) $d - d$ transitions, with a distinct absorption peak at 1.83 eV. This is assigned to the lowest energy chromium $d - d$ transition ($^4A_{2g} \rightarrow {}^4T_{2g}$). This transition occurs at a lower energy than that of the bulk chromium (III) oxide, indicating a change in ligand field strength, which may be accounted for by contrasting between bulk chromium (III) oxide, and the incomplete layer of chromium (III) oxide nanoparticles on the surface of Nb_2O_5, or through incorporation of chromium into the Nb_2O_5 lattice. Although the second visible $d - d$ transition $^4A_{2g}$ to $^4T_{1g}$ is not seen as a distinct maximum in the difference spectrum, the transition will be present in the absorbance. The energy difference between the $^4A_{2g}$ to $^4T_{2g}$ and $^4A_{2g}$ to $^4T_{1g}$ transitions on the Tanabe-Sugano diagram is equivalent for a wide range of Racah B parameters. In order to help differentiate the chromium (III) $^4A_{2g} \rightarrow {}^4T_{1g}$ transition from processes involving both Cr_2O_3 and Nb_2O_5, we assume that the $^4A_{2g}$ to $^4T_{1g}$ transition will occur at an equivalent higher energy to $^4A_{2g}$ to $^4T_{2g}$ in $3\%Cr_2O_3$-Nb_2O_5 as in the bulk Cr_2O_3. This transition is therefore predicted to occur at 2.43 eV in $3\%Cr_2O_3$-Nb_2O_5. The absorbance of both, $d - d$ transitions of the chromium oxide on the surface of niobium oxide can be fitted with Gaussian peaks at fixed energy and variable intensity and width. These modelled peaks are further subtracted from the difference spectrum shown in Figure 3b, leaving just the optical absorption due to interaction between the Cr_2O_3 and Nb_2O_5. The onset of this visible light absorption can be extracted from a plot of $[F(R)xE]^{0.5}$ versus energy which is linear, consistent with an indirect band gap of 2.27 eV (Figure 3c).

This transition could be assigned to oxygen to chromium charge transfer, as well as chromium to niobium, and in order to investigate this possibility we collected X-ray photoelectron spectroscopy data. Valence band photoemission spectra were measured on both $1\%Cr_2O_3$-Nb_2O_5 and $3\%Cr_2O_3$-Nb_2O_5, in addition to Nb_2O_5. (Figure 3d). These show the density of filled states at different binding energies. The Cr doped samples show a feature around 2.3 eV binding energy (figure 3d), situated above the Nb_2O_5 valence band maximum, which increases in intensity with increasing Cr doping. Hence these are assigned as Cr $3d$ states. The binding energy scale of the valence band X-ray photoelectron spectra are set so that zero binding energy corresponds to the Fermi level. In Nb_2O_5, which is an n-type semiconductor, the Fermi level will be located

close to the conduction band minimum, due to the presence of donor states just below the conduction band. Therefore the chromium $3d$ states shown in Figure 3d are approximately 2.3 eV below the conduction band. This matches well with the optical transition of 2.27 eV in these materials, evident from the analysis of the absorption spectra in Figure 3. This transition is therefore assigned as transfer from chromium (III) $3d$ states to the Nb_2O_5 conduction band, consisting predominantly of niobium $4d$ orbitals. This XPS data, in addition to the indirect band gap calculated from the diffuse reflectance of $3\%Cr_2O_3$-Nb_2O_5 is evidence that there is a metal-metal charge transfer transition from the chromium $3d$ orbital to the niobium $4d$ orbital, at 2.27 eV.

3.4 Methyl orange photocatalysis

The photo-oxidation of the azo dye methyl orange can be used as a probe for photocatalysis reactions.[24, 25] Visible light photocatalysis of the degradation of methyl orange was performed at pH 3.5 in water. This pH was selected to combine a negative zeta potential for the photocatalyst suspension (−6.29 mV) with the formation of the protonated form of methyl orange and thus ensure good adsorption of the dye on the catalyst. Control reactions were performed using Nb_2O_5 with visible light and $5\%Cr_2O_3$-SiO_2 with a surface area of 90 m^2 g^{-1} (prepared using the protocol including washing steps for the Nb_2O_5 composite) (Figure S7). As silica has a band gap of 9 eV,[26] a charge transfer of chromium to silicon comparable to the chromium (III) − niobium (V) interaction

Fig. 3 (a) Diffuse reflectance of Nb_2O_5, chromium (III) oxide (Cr_2O_3) and $3\%Cr_2O_3$-Nb_2O_5. (b) Diffuse reflectance spectra showing the measured difference between the $3\%Cr_2O_3$-Nb_2O_5 and Nb_2O_5, spectra ([$3\% Cr_2O_3$-Nb_2O_5] − [Nb_2O_5]), the fitted Cr_2O_3 absorbance emanating from $3\%Cr_2O_3$-Nb_2O_5, and the chromium − niobium visible interaction of $3\% Cr_2O_3$-Nb_2O_5, determined from the subtraction of both the fitted
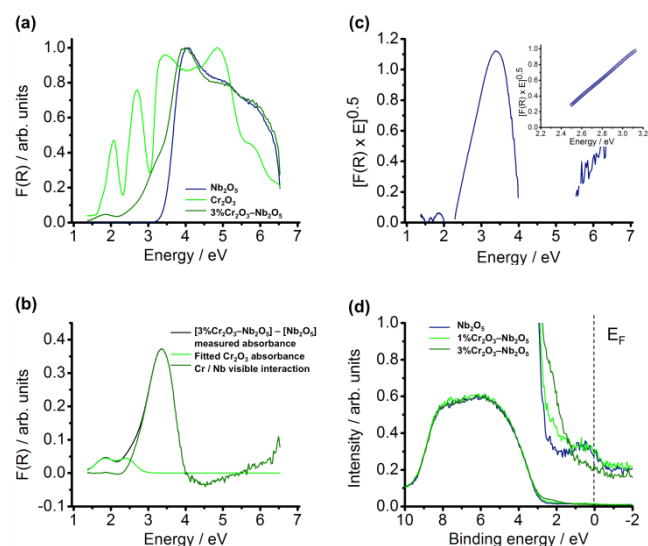
Cr_2O_3 absorbance, and the niobium oxide absorbance. (c) The chromium − niobium visible interaction of $3\% Cr_2O_3$-Nb_2O_5 plotted as an indirect band gap diagram (insert) The extrapolation of the linear section of the spectrum to determine the intercept of the x-axis, hence the indirect band gap, calculated to 2.27 eV, with R2=0.999. (d) Valence band XPS spectra for Nb_2O_5, $1\% Cr_2O_3$-Nb_2O_5 and $3\% Cr_2O_3$-Nb_2O_5. Insert shows the binding energy from 2.5 eV to -2 eV at 20x magnification.

would not be expected, and the diffuse reflectance of 5%Cr_2O_3-SiO_2 confirms this to be the case (Figure S8). The visible light region of the diffuse reflectance of 5%Cr_2O_3-SiO_2 is comparable to that of bulk Cr_2O_3, with $d-d$ transitions present in the visible region, and the LMCT present in the UV region; the silica electronic transitions being outside the range of the UV/Vis instrument measurement. No evidence of interaction between the chromium and the silicon can be observed from the diffuse reflectance spectra. It can be seen that in both control reactions, the concentration of methyl orange remains constant over the course of the reaction (Figure S7).

Visible light irradiation of aqueous methyl orange in the presence of the 5%Cr_2O_3-Nb_2O_5 composite decreases the concentration of methyl orange (Figure 4a) according to first order kinetics (Figure S9). The reaction rate is maximized at 2.0 g L^{-1} of catalyst as this corresponds to maximal light absorption. Visible light irradiation of methyl orange in the presence of 5%Cr2O3-Nb_2O_5 at neutral pH decreases the concentration of methyl orange, but to a lesser extent compared to the solution at pH 3.5, due to the limited adsorption of methyl orange onto the surface of the material at neutral pH (Figure S10). Methyl orange degradation reactions carried out using band pass filters in front of the xenon lamp, centred on 400 nm and 450 nm reveal enhanced activity at 400 nm (Figure 4b).
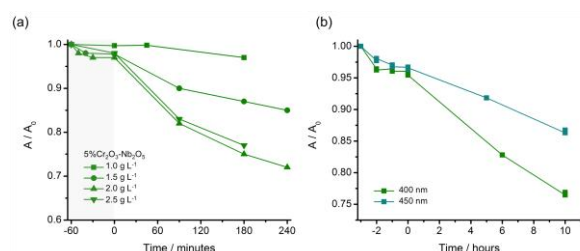

Fig 4: (a) The change in concentration of the red form of methyl orange over the course of a reaction of 5%Cr_2O_3-Nb_2O_5 at concentrations of 1 g L^{-1} to 2.5 g L^{-1} under visible light. (b) Change in concentration of methyl orange with the 5%Cr_2O_3–Nb_2O_5 composite reacted under the xenon lamp with a 400nm, and a 450 nm band pass filter

3.5 Discussion

The combination of spectroscopies used allows the schematic diagram in Figure 5a for the sequence of optical transitions present in the 3%Cr_2O_3-Nb_2O_5 composite to be derived in terms of the chromium $d-d$ transitions, the niobium oxide band gap transition and the metal-to-metal charge transfer.

The 2.27 eV transition is assigned to transfer of electrons from the localised Cr^{3+} t_{2g} states into the niobium 4d-derived conduction band, as all the other transitions can be accounted for based on the properties of the component materials. This is the only transition that produces delocalised charge carriers that takes place in the visible region, and is thus a candidate for visible light photocatalytic activity. The activity will be degraded by recombination due to the excited term states derived from Cr^{3+}. The photogenerated t_{2g} hole is expected to be strongly covalent with oxygen and have some delocalised character. The $d-d$ transitions do not generate delocalised carriers and are thus expected to be inactive for photocatalysis

despite generating absorption in the visible range. Consistent with this, the control measurements on Nb_2O_5 and on Cr_2O_3 supported on SiO_2 show that Nb_2O_5 and Cr_2O_3 in isolation do not photocatalytically degrade methyl orange with visible light. The wavelength dependence of the visible light activity of the composite can be seen by the action spectra produced when the data compiled in the methyl orange reaction using band pass filters (Figure 6); this shows the visible light activity accurately tracks the part of the composite absorption spectrum that has been directly assigned to the Cr to Nb charge transfer (Figure 6a). This supports the procedure used to isolate the MMCT contribution to the visible light absorption. As this is not a sensitized reaction, we can speculate the reaction takes place via both hydroxyl groups that are produced by the hole, and superoxide anions formed from the oxygen in solution and the photogenerated electron.
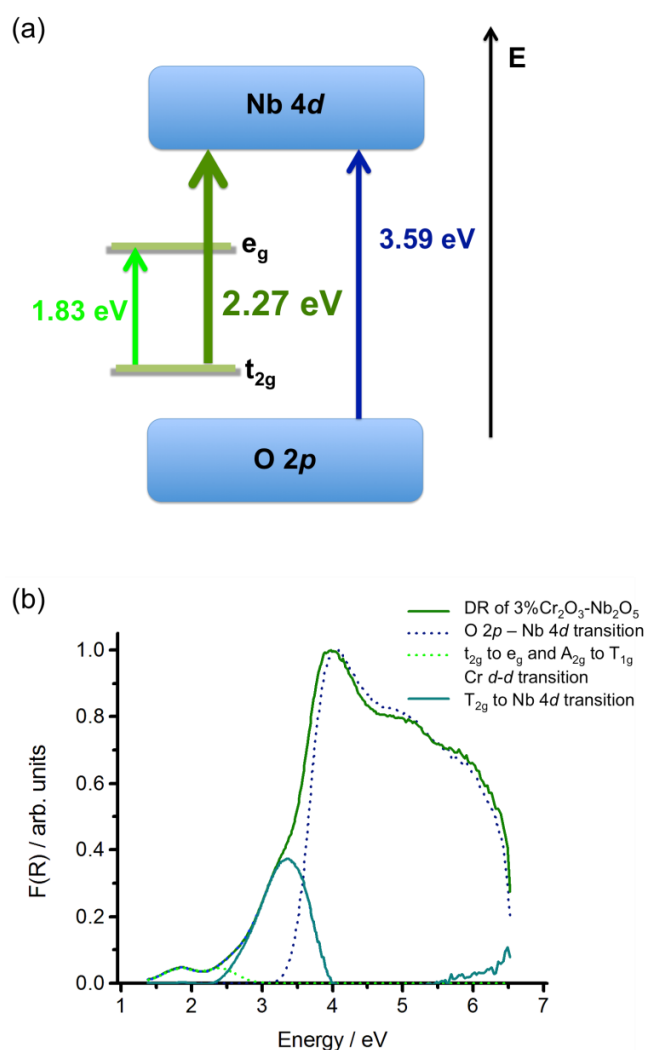

Fig 5 (a) A diagram representing the electronic structure of 3%Cr_2O_3-Nb_2O_5. (b) The electronic transitions identified on the diffuse reflectance of 3%Cr_2O_3-Nb_2O_5

It is interesting to note that before the calcination, the diffuse reflectance of the nitrate-impregnated material does not show any clear interaction between chromium (III) and niobium (V) in the composite. This is noticeably different from the

6 | *J. Mater. Chem. C*, 2015, **00**, 1-3

This journal is © The Royal Society of Chemistry 20xx

chromium (III) – titanium (IV) oxide material synthesised by the Hashimoto group, who identify Cr^{3+}/Ti^{4+} interaction on material that has not been calcined.[9, 10] In the Cr/Nb case reported here, the combined XPS and diffuses reflectance analysis shows that formation of oxide species is important to produce the charge transfer interaction required for photocatalysis in the visible region.

charge-transfer absorbance identified. This demonstrates that Cr/Nb charge transfer can be an effective route to photocatalysis. At the same time this material can absorb visible light in metal centred Cr^{3+} $d - d$ transitions that are not effective for photocatalysis. This illustration provides an insight into the conventions for photocatalysis and can help in the design of future photocatalytic composite materials.
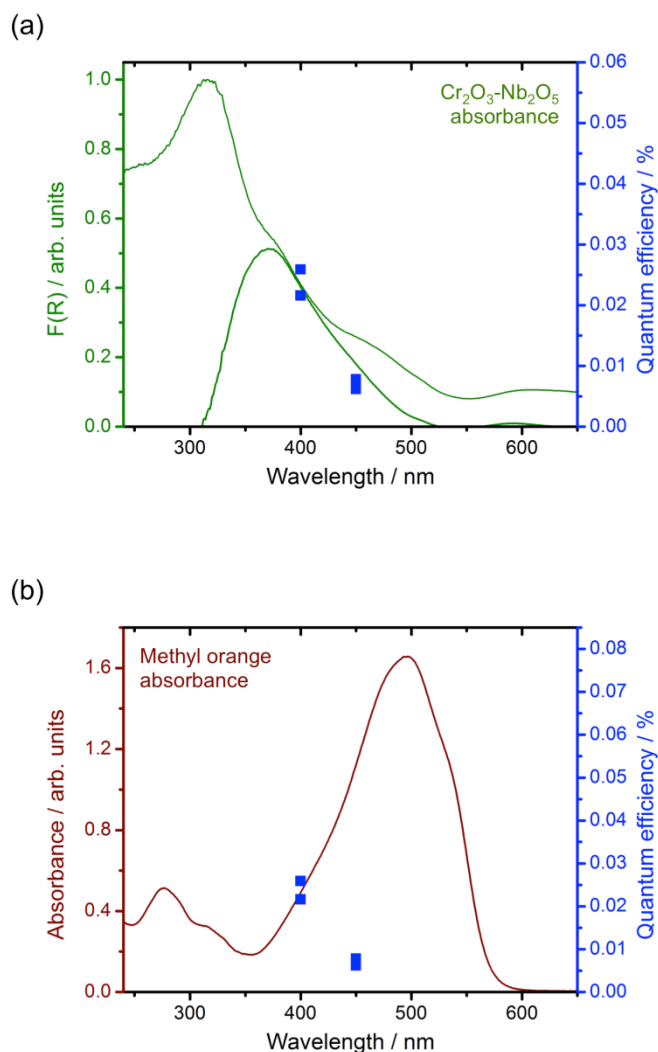
(a)

(b)

Fig 6 (a) Quantum efficiency of 5%Cr_2O_3–Nb_2O_5 visible light reaction with methyl orange overlaid with the diffuse reflectance of 5%Cr_2O_3–Nb_2O_5. The lower curve is the part of the overall absorption assigned purely to the Cr/Nb MMCT interaction. (b) Quantum efficiency of the 5%Cr_2O_3–Nb_2O_5 visible light reaction with methyl orange overlaid with the absorbance spectrum of methyl orange.

Conclusions

We have synthesized and characterized a composite structure of Cr_2O_3-Nb_2O_5 which shows clear absorption bands in the visible spectrum that can be assigned to chromium – niobium charge transfer transitions, further verified by valance band XPS. These visible interactions can be used to absorb light and catalyse the breakdown of a model dye – methyl orange, with the efficiency of the photocatalytic reaction reflecting the

Acknowledgements

References

1. M. R. Hoffmann, S. T. Martin, W. Y. Choi and D. W. Bahnemann, *Chem Rev*, 1995, **95**, 69-96.
2. A. Mills and S. LeHunte, *J. Photochem. Photobiol., A*, 1997, **108**, 1-35.
3. A. Kudo and Y. Miseki, *Chemical Society Reviews*, 2009, **38**, 253-278.
4. H. J. Zhang, G. H. Chen and D. W. Bahnemann, *Journal of Materials Chemistry*, 2009, **19**, 5089-5121.
5. J. S. Lee, *Catal. Surv. Asia*, 2005, **9**, 217-227.
6. F. E. Osterloh, *Chem. Mater.*, 2008, **20**, 35-54.
7. F. E. Osterloh, *Chemical Society Reviews*, 2013, **42**, 2294-2320.
8. W. Y. Lin and H. Frei, *J Am Chem Soc*, 2005, **127**, 1610-1611.
9. H. Irie, S. Miura, R. Nakamura and K. Hashimoto, *Chem Lett*, 2008, **37**, 252-253.
10. H. Irie, T. Shibanuma, K. Kamiya, S. Miura, T. Yokoyama and K. Hashimoto, *Appl Catal B-Environ*, 2010, **96**, 142-147.
11. J. H. Clark, M. S. Dyer, R. G. Palgrave, C. P. Ireland, J. R. Darwent, J. B. Claridge and M. J. Rosseinsky, *J. Am. Chem. Soc.*, 2011, **133**, 1016-1032.
12. Y. Xu and M. A. A. Schoonen, *Am Mineral*, 2000, **85**, 543-556.
13. H. Kominami, K. Oki, M. Kohno, S. Onoue, Y. Kera and B. Ohtani, *J Mater Chem*, 2001, **11**, 604-609.
14. X. Y. Chen, T. Yu, X. X. Fan, H. T. Zhang, Z. S. Li, J. H. Ye and Z. G. Zou, *Appl Surf Sci*, 2007, **253**, 8500-8506.
15. A. G. S. Prado, E. A. Faria, J. R. SouzaDe and J. D. Torres, *J Mol Catal a-Chem*, 2005, **237**, 115-119.
16. E. A. Faria and A. G. S. Prado, *React Funct Polym*, 2007, **67**, 655-661.
17. A. G. S. Prado, L. B. Bolzon, C. P. Pedroso, A. O. Moura and L. L. Costa, *Appl Catal B-Environ*, 2008, **82**, 219-224.
18. S. X. Ge, H. M. Jia, H. X. Zhao, Z. Zheng and L. Z. Zhang, *J. Mater. Chem.*, 2010, **20**, 3052-3058.
19. X. Wang, G. Chen, C. Zhou, Y. G. Yu and G. Wang, *Eur. J. Inorg. Chem.*, 2012, DOI: 10.1002/ejic.201101285, 1742-1749.

20. C. G. Hatchard and C. A. Parker, *Proc R Soc Lon Ser-A*, 1956, **235**, 518-536.

21. Y.-C. Xie and Y.-Q. Tang, *Advances in Catalysis*, 1990, **37**, 1-43.

22. M. C. Fournier-Salaun and P. Salaun, *Cent Eur J Chem*, 2007, **5**, 1084-1093.

23. S. H. Shen and L. J. Guo, *Catal Today*, 2007, **129**, 414-420.

24. G. T. Brown and J. R. Darwent, *J. Phys. Chem.*, 1984, **88**, 4955-4959.

25. K. Rajeshwar, M. E. Osugi, W. Chanmanee, C. R. Chenthamarakshan, M. V. B. Zanoni, P. Kajitvichyanukul and R. Krishnan-Ayer, *J. Photochem. Photobiol., C*, 2008, **9**, 171-192.

26. R. B. Laughlin, *Phys Rev B*, 1980, **22**, 3021-3029.